

Massive Dirac Fermion at the Surface of the van der Waals Antiferromagnet MnBi_2Te_4

R. C. Vidal,¹ H. Bentmann,^{1,*} T. R. F. Peixoto,¹ A. Zeugner,² S. Moser,^{3,4} C. H. Min,¹ S. Schatz,¹ K. Kißner,¹ M. Ünzelmann,¹ C. I. Fornari,¹ H. B. Vasili,⁵ M. Valvidares,⁵ K. Sakamoto,⁶ J. Fujii,⁷ I. Vobornik,⁷ T. K. Kim,⁸ R. J. Koch,³ C. Jozwiak,³ A. Bostwick,³ J. D. Denlinger,³ E. Rotenberg,³ J. Buck,⁹ M. Hoesch,⁹ F. Diekmann,¹⁰ S. Rohlf,¹⁰ M. Kalläne,^{10,11} K. Rossnagel,^{9,10,11} M. M. Otrokov,^{12,13} E. V. Chulkov,^{13,14,15,16} M. Ruck,^{2,17} A. Isaeva,^{18,19} and F. Reinert¹

¹*Experimentelle Physik VII and Würzburg-Dresden Cluster of Excellence ct.qmat, Universität Würzburg, Am Hubland, D-97074 Würzburg, Germany*

²*Technische Universität Dresden, Department of Chemistry and Food Chemistry, Helmholtzstraße 10, D-01069 Dresden, Germany*

³*Advanced Light Source, Lawrence Berkeley National Laboratory, Berkeley, CA 94720, USA*

⁴*Experimentelle Physik IV and Würzburg-Dresden Cluster of Excellence ct.qmat, Universität Würzburg, Am Hubland, D-97074 Würzburg, Germany*

⁵*ALBA Synchrotron Light Source, E-08290 Cerdanyola del Valles, Spain*

⁶*Department of Materials Science, Chiba University, Chiba 263-8522, Japan*

⁷*Istituto Officina dei Materiali (IOM)-CNR, Laboratorio TASC, Trieste 34149, Italy*

⁸*Diamond Light Source, Harwell Campus, Didcot OX11 0DE, United Kingdom*

⁹*Deutsches Elektronen-Synchrotron DESY, Hamburg, Germany*

¹⁰*Institut für Experimentelle und Angewandte Physik, Christian-Albrechts-Universität zu Kiel, 24098 Kiel, Germany*

¹¹*Ruprecht Haensel Laboratory, Kiel University and DESY, Germany*

¹²*Centro de Física de Materiales (CFM-MPC), Centro Mixto CSIC-UPV/EHU, 20018 Donostia-San Sebastián, Basque Country, Spain*

¹³*IKERBASQUE, Basque Foundation for Science, 48011 Bilbao, Basque Country, Spain*

¹⁴*Departamento de Física de Materiales UPV/EHU, 20080 Donostia-San Sebastián, Basque Country, Spain*

¹⁵*Donostia International Physics Center (DIPC), 20018 Donostia-San Sebastián, Basque Country, Spain*

¹⁶*Saint Petersburg State University, 198504 Saint Petersburg, Russia*

¹⁷*Würzburg-Dresden Cluster of Excellence ct.qmat, Technische Universität Dresden, Helmholtzstraße 10, D-01069 Dresden, Germany*

¹⁸*Leibniz-Institut für Festkörper- und Werkstoffforschung Dresden, Institut für Festkörperforschung, D-01069 Dresden, Germany*

¹⁹*Institut für Festkörper- und Materialphysik, Technische Universität Dresden, D-01062 Dresden, Germany*

(Dated: April 22, 2022)

The layered van der Waals compound MnBi_2Te_4 has been predicted to combine the band ordering of archetypical topological insulators like Bi_2Te_3 with the magnetism of Mn, making this material a viable candidate for the realization of various magnetic topological states. We have systematically investigated the surface electronic structure of $\text{MnBi}_2\text{Te}_4(0001)$ single crystals by use of angle-resolved photoelectron spectroscopy (ARPES) experiments. Combining photon-energy-dependent and spin-resolved measurements we establish the presence of a single massive Dirac fermion at the $\text{MnBi}_2\text{Te}_4(0001)$ surface, both, in the low-temperature antiferromagnetic phase and in the paramagnetic phase. Our experimental results establish the coexistence of a topological surface state and magnetic order in MnBi_2Te_4 .

The hallmark of a topological insulator is a single spin-polarized Dirac cone at the surface which is protected by time reversal-symmetry and originates from a band inversion in the bulk [1, 2]. Notably, breaking time-reversal symmetry by magnetic order does not necessarily destroy the non-trivial topology but instead may drive the system into another topological phase. One example is the quantum anomalous Hall (QAH) state that has been observed in magnetically doped topological insulators [3]. The QAH state, in turn, may form the basis for yet more exotic electronic states, such as axion insulators [4, 5] and chiral Majorana fermions [6]. Another example is the antiferromagnetic topological insulator state

which is protected by a combination of time-reversal and lattice translational symmetries [7].

Magnetic order in a topological insulator has mainly been achieved by doping with 3d impurities [3, 9], which however inevitably gives rise to increased disorder. By contrast, the layered van der Waals material MnBi_2Te_4 [8, 10] has recently been proposed to realize an intrinsic magnetic topological insulator [11–14], i.e. a compound that features magnetic order and a topologically non-trivial bulk band structure at the same time. MnBi_2Te_4 is isostructural to the known topological insulators GeBi_2Te_4 [15–17] and PbBi_2Te_4 [18], but the substitution of Ge or Pb by Mn introduces local magnetic moments

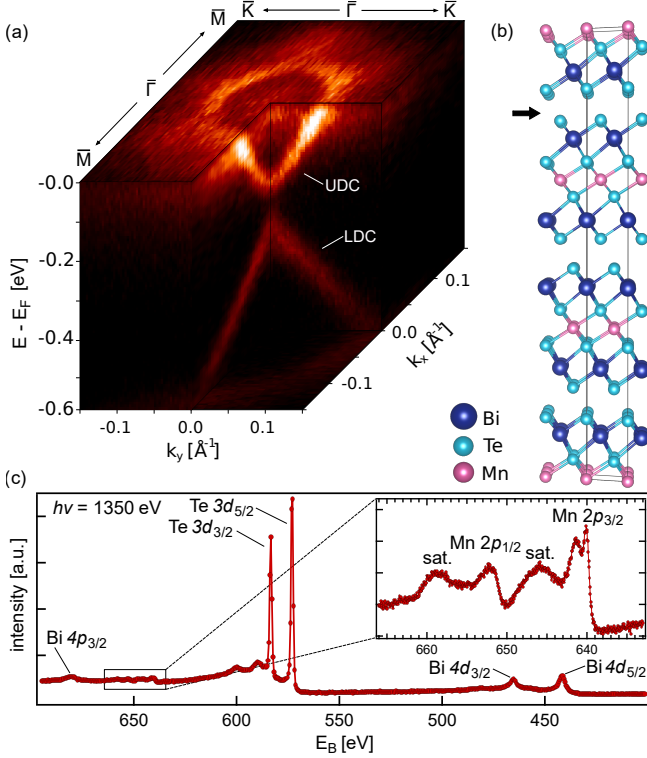


FIG. 1: (color online) (a) ARPES data set for $\text{MnBi}_2\text{Te}_4(0001)$ around the $\bar{\Gamma}$ -point, showing a massive Dirac state with an energy splitting of ca. 100 meV between the upper and the lower Dirac cone (UDC and LDC) [$T = 80$ K, $h\nu = 21.5$ eV]. (b) Crystal structure of MnBi_2Te_4 along one unit cell (black lines) according to Ref. [8]. The black arrow indicates the van der Waals-gap between two septuple layers as the natural cleavage plane. (c) X-ray photoemission spectrum showing core level lines of Mn, Bi and Te.

which order antiferromagnetically below ~ 24 K [11, 19–21]. The resulting interplay of magnetic order and topology in a single compound has been proposed as a promising platform for the realization of a variety of magnetic topological states [11–14, 22].

In this work we present a systematic investigation of the surface electronic structure in $\text{MnBi}_2\text{Te}_4(0001)$ single crystals employing angle-resolved photoelectron spectroscopy (ARPES), spin-resolved ARPES and resonant photoemission at the Mn L -edge. Our measurements reveal a surface state in the bulk band gap that forms a spin-polarized massive Dirac cone in agreement with recent theoretical predictions [11–13]. The large mass-induced gap of ~ 100 meV is robust across the transition from the antiferromagnetic phase into the paramagnetic phase, which we distinguish by X-ray magnetic circular and linear dichroism (XMCD and XMLD) experiments. Our results establish the existence of a topologically non-trivial surface state in a pristine, magnetic compound, and corroborate that MnBi_2Te_4 realizes an intrinsically magnetic topological insulator.

The ARPES measurements were performed at the MAESTRO [Fig. 1(a), 2(a)–(e), Fig. S2] and Merlin [Fig. 4(c)] endsta-

tions of the Advanced Light Source (USA) as well as at beamline I05 of the Diamond Light Source (UK) [Fig. 3(a)–(b)]. The energy resolution of the ARPES experiments was better than 20 meV. Spin-resolved ARPES measurements were performed at the APE beamline of the Elettra synchrotron by use of a Scienta DA30 hemispherical analyser combined with a spin polarimeter based on very low-energy electron diffraction (Sherman function $S = 0.3$). We acquired XMCD and XMLD data in total electron yield (TEY) mode at the BOREAS beamline of the ALBA Synchrotron (Spain). Resonant soft X-ray photoemission data and Mn $2p$ core-level spectra were collected at the ASPHERE III endstation at beamline P04 of PETRA III (Germany) with an energy resolution of ca. 25 meV. Platelet-like MnBi_2Te_4 single crystals were obtained via an optimized crystal-growth procedure as described in Ref. [19].

MnBi_2Te_4 crystallizes in a trigonal lattice (the ordered GeAs_2Te_4 structure type) with septuple [Te-Bi-Te-Mn-Te-Bi-Te] layers stacked in the ABC fashion [8]. The septuple layers are separated by a van der Waals gap, as shown in Fig. 1(b). Our X-ray single-crystal study confirms the structure motif plus a certain degree of Mn/Bi antisite intermixing in both cation positions [19]. Mn atoms are ordered in definite crystallographic sites in a periodic crystal lattice in contrast to doped topological insulators. Cleavage of single crystals exposes well-ordered (0001) surfaces suitable for surface sensitive experiments. From an inspection of the Mn $2p$ core-level line shapes in X-ray photoemission and absorption (XPS and XAS) in Fig. 1(c) and Fig. S1 we infer a $3d^5$ configuration of the Mn ions (Mn^{2+}) [23, 24]. Magnetic susceptibility measurements of bulk MnBi_2Te_4 imply an antiferromagnetic ground state below $T_N = 24$ K [11, 19–21]. Furthermore, they indicate an out-of-plane orientation of the magnetic moments with ferromagnetic intralayer coupling and antiferromagnetic interlayer coupling. This is in agreement with first-principles calculations [11, 13] and fully supported by our XMCD and XMLD measurements [see Fig. S1 in the supplemental material].

Figure 1(a) presents an ARPES data set for $\text{MnBi}_2\text{Te}_4(0001)$ close the Fermi level E_F . The data bear strong similarities to those obtained previously for isostructural $\text{GeBi}_2\text{Te}_4(0001)$ [15–17], and show a state with Dirac-like band dispersion at the $\bar{\Gamma}$ -point, see also Figs. 2 and 3. In contrast to $\text{GeBi}_2\text{Te}_4(0001)$, however, our data provide evidence for an energy splitting between the upper and the lower part of the Dirac cone (UDC and LDC). The measured dispersion in Fig. 1(a), including the size of the splitting of ~ 100 meV at $\bar{\Gamma}$, is in good agreement with previous first-principles theory for antiferromagnetic $\text{MnBi}_2\text{Te}_4(0001)$ [11, 13] and for a single, ferromagnetic MnBi_2Te_4 septuple layer on $\text{Bi}_2\text{Te}_3(0001)$ [25]. These calculations predict the presence of a spin-polarized Dirac surface state with a gap in the magnetically ordered state.

A more detailed analysis of the electronic band structure is presented in Figs. 2(a)–(c). Besides the UDC, which shows a narrow line shape typical for surface states, we observe

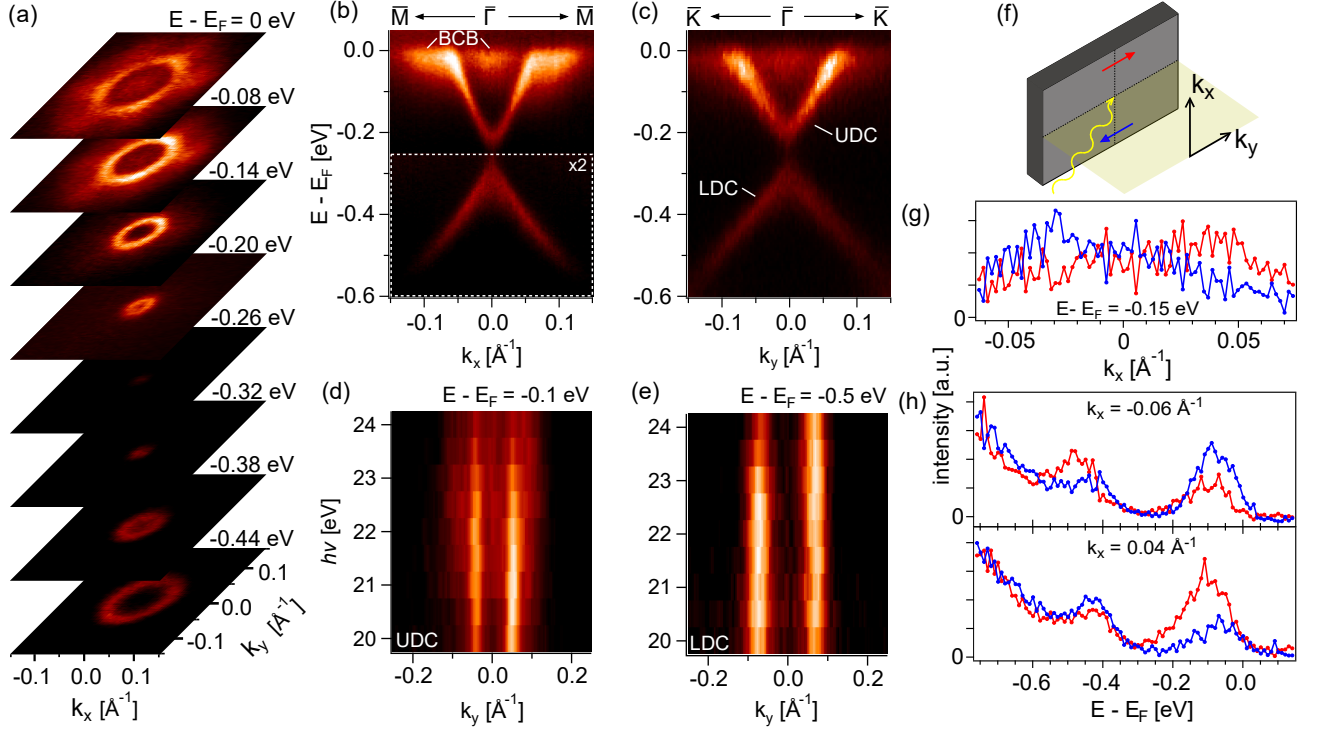


FIG. 2: (color online) (a) ARPES constant energy contours for MnBi₂Te₄(0001). At the Fermi level a hexagonal warping of the UDC and a flower-like pattern of the bulk conduction band (BCB) is observed. (b)-(c) ARPES data sets along the $\bar{\Gamma}\bar{M}$ - and $\bar{\Gamma}\bar{K}$ -directions. (d)-(e) Photon-energy-dependent data for the UDC and LDC ($T = 18$ K). (f) Schematic of the experimental geometry for the spin-resolved measurements. (g)-(h) Spin-resolved momentum- and energy distribution curves obtained for a spin-quantization axis along y , i.e. in-plane and perpendicular to the probed wave vector along k_x . The reversal of the spin polarization of the UDC at $\pm k_x$ indicates a helical spin configuration. All data sets except for (d)-(e) were acquired with $h\nu = 21.5$ eV and at $T = 80$ K.

more diffuse features close to the Fermi level which we attribute to the bottom of the bulk conduction band (BCB). One BCB feature is centered at the $\bar{\Gamma}$ -point in between the UDC branches, which has been observed similarly in n-doped topological insulators like Bi₂Te₃ [26]. Furthermore, we find additional BCB features at finite wave vectors along the $\bar{\Gamma}\bar{M}$ direction which form a flower-like pattern in the Fermi surface and partly overlap with the UDC. This characteristic shape of the conduction band minimum poses an important constraint for theoretical approaches. We note that similar pockets at finite wave vectors along $\bar{\Gamma}\bar{M}$ have been observed for GeBi₂Te₄(0001) [17].

In order to investigate the dimensionality of the massive Dirac state we performed photon-energy-dependent ARPES measurements [Fig. 2(d)-(e) and Fig. S2 in the supplement]. We find that the dispersion of the UDC and the LDC both show no significant variation over the measured photon-energy range between $h\nu = 20$ -24 eV. While generally this observation is consistent with a surface origin of these features, we note that, according to previous calculations, also the bulk states at the valence band maximum and the conduction band minimum have a markedly two-dimensional character with very small dispersion along k_z [11–13]. Although this hampers an unambiguous assignment, comparing our data to the calculated band structure [11] suggests a surface origin of the UDC and

a mixed surface and bulk-valence-band character of the LDC. This situation is reminiscent of related topological insulators like Bi₂Se₃ [27].

A key property of the Dirac surface state in a topological insulator is a high degree of spin polarization. Our spin-resolved ARPES data in Fig. 2(g)-(h) indeed confirm a spin polarization of the UDC. As sketched in Fig. 2(f), the spin-polarized data were obtained at wave vectors along k_x with a spin-quantization axis along y . The p-polarized light was incident in the yz plane. In particular, the energy distribution curve at $k_x = 0.04$ Å⁻¹ in Fig. 2(h) provides evidence for a high spin polarization of the UDC. At $k_x = -0.06$ Å⁻¹ the spin polarization of the UDC is reversed as expected for a spin-momentum-locked state, but also significantly reduced. We attribute the reduction in spin polarization at this wave vector to a stronger overlap and potentially hybridization of the UDC with the BCB. The reversal of the spin polarization at $\pm k_x$ is also observed in the spin-resolved momentum distribution curve in Fig. 2(g).

Collectively, these results provide strong experimental evidence for a spin-polarized massive Dirac state at the surface of MnBi₂Te₄(0001). To study the origin of the splitting of the Dirac cone, we compare ARPES data sets obtained below and above the antiferromagnetic ordering temperature $T_N = 24$ K

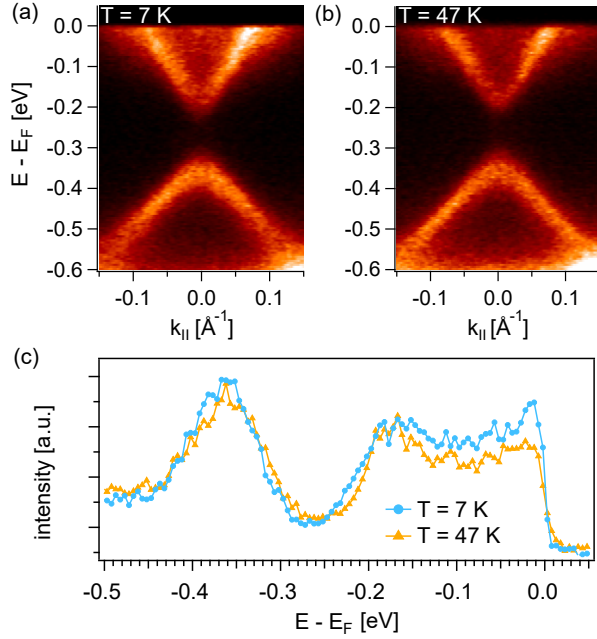


FIG. 3: (color online) (a)-(b) Temperature-dependent ARPES data for $\text{MnBi}_2\text{Te}_4(0001)$ below and above T_N measured with $h\nu = 21.5$ eV along $\bar{\Gamma}\bar{M}$. (c) Energy distribution curves (EDC) at $k_{\parallel} = 0$.

in Fig. 3. Apparently, the dispersion shows no pronounced changes when passing from the antiferromagnetic into the paramagnetic state. The EDC taken at the $\bar{\Gamma}$ point suggest a slight shift of both the UDC and LDC to higher binding energy for lower T , but there is no significant change in the size of the splitting above T_N .

The lack of a temperature dependence up to substantially above T_N indicates that the splitting of the Dirac cone does not originate from long-range magnetic order with out-of-plane magnetization, as was expected based on previous calculations for MnBi_2Te_4 [12, 13, 25, 28] and other materials [29–32]. However, the paramagnetic state has not been considered in these works. Despite this discrepancy we note that the size of the measured splitting is of similar magnitude as those predicted theoretically for magnetically ordered MnBi_2Te_4 [11–13]. This suggests that the coupling strength between the surface state and the magnetic moments of Mn is generally sufficient to induce a splitting of up to 100 meV as observed experimentally. We note that also in other systems a gap in the Dirac cone was observed in the paramagnetic regime, including Fe- and Mn-doped Bi_2Se_3 [9, 33, 34]. Similar findings were also obtained for $\text{TlBi}(\text{Se}_x\text{S}_{1-x})_2$ [35].

Overall, our finding of a massive Dirac cone on the $\text{MnBi}_2\text{Te}_4(0001)$ surface is in agreement with several first-principles theory studies, which unanimously predict that the bulk band structure of MnBi_2Te_4 [11–13] and also MnBi_2Se_4 [36, 37] is topologically non-trivial. A potential concern here is that an accurate description of the localized Mn $3d$ orbitals is not readily expected in calculations based on density functional theory (DFT) and could play an essential role [38].

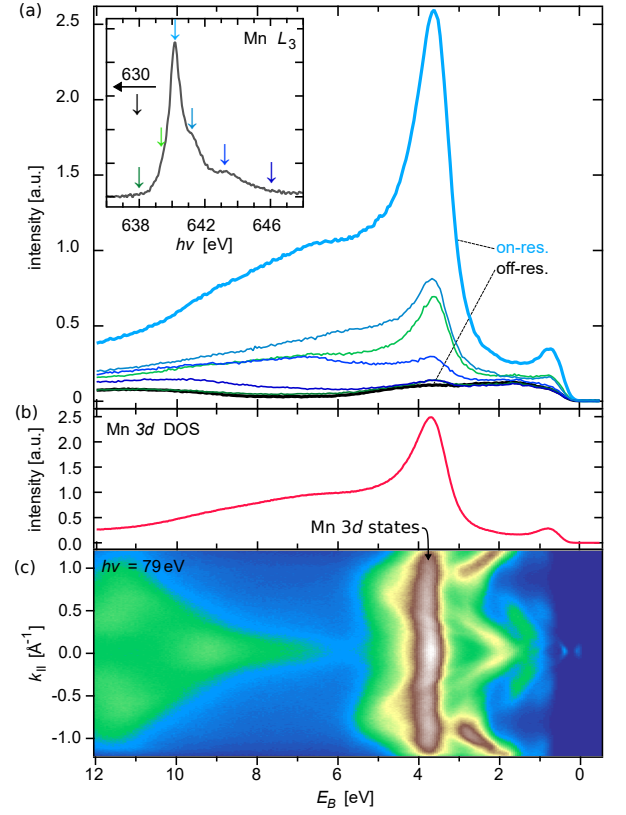


FIG. 4: (color online) (a) Valence band spectra for $\text{MnBi}_2\text{Te}_4(0001)$ obtained by resonant excitation at photon energies $h\nu$ near the Mn $2p \rightarrow 3d$ absorption edge. The inset shows the Mn L_3 absorption edge with colored arrows indicating the corresponding excitation energies. (b) Difference of the spectra measured under on- (light blue) and off-resonant (black) conditions, showing the contribution of the Mn $3d$ states to the valence band. (c) Angle-resolved valence band spectrum measured with $h\nu = 79$ eV.

To assess the character of the Mn $3d$ states we have carried out resonant photoemission experiments at the $L_{2,3}$ absorption edge [Fig. 4]. The measured Mn density of states (DOS) shows a state at ca. 3.8 eV and another one at ca. 0.8 eV that is attributed to hybridization between Mn $3d$ and Te $5p$ orbitals near the top of the valence band, which is in rather good agreement with DFT [8]. This result suggests that these calculations capture the energetics of the Mn $3d$ states reasonably well and thus substantiates the topological classification.

The persistence of the gap above T_N , however, calls for further theoretical investigation. In general, the protection of the Dirac point in a topological insulator is based on the absence of backscattering due to destructive interference between scattering channels related by time-reversal symmetry. A recent theory shows that, if this destructive interference is perturbed, strong impurity scattering may induce gap features at the Dirac point of similar size as observed here for MnBi_2Te_4 [39]. Notably, single magnetic Mn impurities placed in the topological insulator Bi_2Te_3 have been found to constitute strong scattering centers for the topological surface state [40].

Therefore, based on our results we anticipate that the local magnetic moments in the Mn layers in MnBi_2Te_4 may allow for backscattering processes and thereby destroy the topological protection of the Dirac point. A rather local nature of the Mn states in MnBi_2Te_4 is supported by the measured $3d$ DOS in Fig. 4 that resembles the one of single Mn impurities in Sb_2Te_3 [41].

In summary, our experiments unveil a topologically non-trivial surface electronic structure of the antiferromagnet $\text{MnBi}_2\text{Te}_4(0001)$. In particular, MnBi_2Te_4 provides a first instance of a material that features a massive Dirac surface state and relies neither on doping nor alloying. Our results could provide new pathways to exploit the interplay of antiferromagnetism and topological edge states in spintronic device concepts based on the emerging material class of van der Waals magnets [42].

ACKNOWLEDGMENTS

We acknowledge financial support from the DFG through SFB1170 'Tocotronics', SFB1143 'Correlated Magnetism', SPP 1666 'Topological insulators', ERA-Chemistry Programm (RU-776/15-1), and the Würzburg-Dresden Cluster of Excellence on Complexity and Topology in Quantum Matter – *ct.qmat* (EXC 2147, project-id 39085490). We also acknowledge the support by Spanish Ministerio de Economía y Competitividad (MINECO Grant No. FIS2016-75862-P), Academic D.I. Mendeleev Fund Program of Tomsk State University (Project No. 8.1.01.2018), the Saint Petersburg State University grant for scientific investigations (Grant No. 15.61.202.2015), and Russian Foundation for Basic Research (Grant No. 18-52-06009). S.M. acknowledges support by the Swiss National Science Foundation (Grant No. P300P2-171221). This research used resources of the Advanced Light Source, which is a DOE Office of Science User Facility under contract no. DE-AC02-05CH11231. We acknowledge Diamond Light Source for access to beamline I05 (proposals no. SI19278) that contributed to the results presented here. This work has been partly performed in the framework of the Nanoscience Foundry and Fine Analysis (NFFA-MIUR, Italy) facility.

* Electronic address: Hendrik.Bentmann@physik.uni-wuerzburg.de

- [1] M. König, S. Wiedmann, C. Brüne, A. Roth, H. Buhmann, L. W. Molenkamp, X. Qi, and S. Zhang, *Science* **318**, 766 (2007).
- [2] M. Z. Hasan and C. L. Kane, *Rev. Mod. Phys.* **82**, 3045 (2010).
- [3] C.-Z. Chang, J. Zhang, X. Feng, J. Shen, Z. Zhang, M. Guo, K. Li, Y. Ou, P. Wei, L.-L. Wang, et al., *Science* **340**, 167 (2013).
- [4] M. Mogi, M. Kawamura, R. Yoshimi, A. Tsukazaki, Y. Kozuka, N. Shirakawa, K. S. Takahashi, M. Kawasaki, and Y. Tokura, *Nature Materials* **16**, 516 (2017).
- [5] D. Xiao, J. Jiang, J.-H. Shin, W. Wang, F. Wang, Y.-F. Zhao, C. Liu, W. Wu, M. H. W. Chan, N. Samarth, et al., *Phys. Rev. Lett.* **120**, 056801 (2018).
- [6] Q. L. He, L. Pan, A. L. Stern, E. C. Burks, X. Che, G. Yin, J. Wang, B. Lian, Q. Zhou, E. S. Choi, et al., *Science* **357**, 294 (2017).
- [7] R. S. K. Mong, A. M. Essin, and J. E. Moore, *Phys. Rev. B* **81**, 245209 (2010).
- [8] D. S. Lee, T.-H. Kim, C.-H. Park, C.-Y. Chung, Y. S. Lim, W.-S. Seo, and H.-H. Park, *CrystEngComm* **15**, 5532 (2013).
- [9] Y. L. Chen, J.-H. Chu, J. G. Analytis, Z. K. Liu, K. Igarashi, H.-H. Kuo, X. L. Qi, S. K. Mo, R. G. Moore, D. H. Lu, et al., *Science* **329**, 659 (2010).
- [10] S. V. Eremin, M. M. Otrokov, and E. V. Chulkov, *J. Alloys Compd.* **709**, 172 (2017).
- [11] M. M. Otrokov, I. I. Klimovskikh, H. Bentmann, A. Zeugner, Z. S. Aliev, S. Gaß, A. U. B. Wolter, A. V. Koroleva, D. Estyunin, A. M. Shikin, et al., arXiv:1809.07389 [cond-mat] (2018).
- [12] D. Zhang, M. Shi, K. He, D. Xing, H. Zhang, and J. Wang, arXiv:1808.08014 [cond-mat] (2018).
- [13] J. Li, Y. Li, S. Du, Z. Wang, B.-L. Gu, S.-C. Zhang, K. He, W. Duan, and Y. Xu, arXiv:1808.08608 [cond-mat] (2018).
- [14] Y. Gong, J. Guo, J. Li, K. Zhu, M. Liao, X. Liu, Q. Zhang, L. Gu, L. Tang, X. Feng, et al. (2018), arXiv:1809.07926.
- [15] M. Neupane, S.-Y. Xu, L. A. Wray, A. Petersen, R. Shankar, N. Alidoust, C. Liu, A. Fedorov, H. Ji, J. M. Allred, et al., *Phys. Rev. B* **85**, 235406 (2012).
- [16] K. Okamoto, K. Kuroda, H. Miyahara, K. Miyamoto, T. Okuda, Z. S. Aliev, M. B. Babanly, I. R. Amiraslanov, K. Shimada, H. Namatame, et al., *Phys. Rev. B* **86**, 195304 (2012).
- [17] M. Arita, H. Sato, K. Shimada, H. Namatame, M. Taniguchi, M. Sasaki, M. Kitaura, A. Ohnishi, and H.-J. Kim, in *Proceedings of the 12th Asia Pacific Physics Conference (APPC12)* (Journal of the Physical Society of Japan, 2014), vol. 1 of *JPS Conference Proceedings*.
- [18] S. Souma, K. Eto, M. Nomura, K. Nakayama, T. Sato, T. Takahashi, K. Segawa, and Y. Ando, *Phys. Rev. Lett.* **108**, 116801 (2012).
- [19] A. Zeugner, F. Nietschke, A. U. B. Wolter, S. Gaß, R. C. Vidal, T. R. F. Peixoto, D. Pohl, C. Damm, A. Lubk, R. Hentrich, et al., arXiv:1812.03106 [cond-mat] (2018).
- [20] S. H. Lee, Y. Zhu, Y. Wang, L. Miao, T. Pillsbury, S. Kempinger, D. Graf, N. Alem, C.-Z. Chang, N. Samarth, et al., arXiv:1812.00339 [cond-mat] (2018).
- [21] J.-Q. Yan, Q. Zhang, T. Heitmann, Z. L. Huang, W. D. Wu, D. Vaknin, B. C. Sales, R. J. McQueeney, arXiv:1902.10110 (2019).
- [22] E. D. L. Rienks, S. Wimmer, P. S. Mandal, O. Caha, J. Rika, A. Ney, H. Steiner, V. V. Volobuev, H. Groiss, M. Albu, et al. (2018), arXiv:1810.06238.
- [23] H. Kurata and C. Colliex, *Phys. Rev. B* **48**, 2102 (1993).
- [24] R. Qiao, T. Chin, S. J. Harris, S. Yan, and W. Yang, *Current Applied Physics* **13**, 544 (2013).
- [25] M. M. Otrokov, T. V. Menshchikova, M. G. Vergniory, I. P. Rusinov, A. Y. Vyazovskaya, Y. M. Koroteev, G. Bihlmayer, A. Ernst, P. M. Echenique, A. Arnau, et al., *2D Materials* **4**, 025082 (2017).
- [26] M. Michiardi, I. Aguilera, M. Bianchi, V. E. de Carvalho, L. O. Ladeira, N. G. Teixeira, E. A. Soares, C. Friedrich, S. Blügel, and P. Hofmann, *Phys. Rev. B* **90**, 075105 (2014).
- [27] Y. Xia, D. Qian, D. Hsieh, L. Wray, A. Pal, H. Lin, A. Bansil,

- D. Grauer, Y. S. Hor, R. J. Cava, et al., *Nature Physics* **5**, 398 (2009).
- [28] M. M. Otrokov, T. V. Menshchikova, I. P. Rusinov, M. G. Vergniory, V. M. Kuznetsov, and E. V. Chulkov, *JETP Letters* **105**, 297 (2017).
- [29] Q. Liu, C.-X. Liu, C. Xu, X.-L. Qi, and S.-C. Zhang, *Phys. Rev. Lett.* **102**, 156603 (2009).
- [30] J. Henk, M. Flieger, I. V. Maznichenko, I. Mertig, A. Ernst, S. V. Eremeev, and E. V. Chulkov, *Phys. Rev. Lett.* **109**, 076801 (2012).
- [31] T. Hirahara, S. V. Eremeev, T. Shirasawa, Y. Okuyama, T. Kubo, R. Nakanishi, R. Akiyama, A. Takayama, T. Hajiri, S.-i. Ideta, et al., *Nano Lett.* **17**, 3493 (2017).
- [32] S. V. Eremeev, M. M. Otrokov, and E. V. Chulkov, *Nano Lett.* **18**, 6521 (2018).
- [33] J. Sanchez-Barriga, A. Varykhalov, G. Springholz, H. Steiner, R. Kirchschlager, G. Bauer, O. Caha, E. Schierle, E. Weschke, A. A. Ünal, et al., *Nature Communications* **7**, 10559 (2016).
- [34] M. Brahlek, N. Bansal, N. Koirala, S.-Y. Xu, M. Neupane, C. Liu, M. Z. Hasan, and S. Oh, *Phys. Rev. Lett.* **109**, 186403 (2012).
- [35] T. Sato, K. Segawa, K. Kosaka, S. Souma, K. Nakayama, K. Eto, T. Minami, Y. Ando, and T. Takahashi, *Nature Physics* **7**, 840 (2011).
- [36] J. A. Hagmann, X. Li, S. Chowdhury, S.-N. Dong, S. Rouvimov, S. J. Pookpanratana, K. M. Yu, T. A. Orlova, T. B. Bolin, C. U. Segre, et al., *New Journal of Physics* **19**, 085002 (2017).
- [37] S. Chowdhury, K. F. Garrity, F. Tavazza, arXiv:1811.01863 (2018).
- [38] I. D. Marco, P. Thunström, M. I. Katsnelson, J. Sadowski, K. Karlsson, S. Lebgue, J. Kanski, and O. Eriksson, *Nature Communications* **4**, 2645 (2013).
- [39] H. Liu, H. Jiang, Q.-f. Sun, and X. C. Xie, *Phys. Rev. Lett.* **113**, 046805 (2014).
- [40] P. Sessi, F. Reis, T. Bathon, K. A. Kokh, O. E. Tereshchenko, and M. Bode, *Nature Communications* **5**, 5349 (2014).
- [41] M. F. Islam, C. M. Canali, A. Pertsova, A. Balatsky, S. K. Mahatha, C. Carbone, A. Barla, K. A. Kokh, O. E. Tereshchenko, E. Jiménez, et al., *Phys. Rev. B* **97**, 155429 (2018).
- [42] C. Gong and X. Zhang, *Science* **363**, eaav4450 (2019).